European Journal of Cell Biology 101 (2022) 151230

Contents lists available at ScienceDirect

European Journal of Cell Biology

journal homepage: www.elsevier.com/locate/ejcb

Iron metabolism in the social amoeba *Dictyostelium discoideum*: A role for ferric chelate reductases

Barbara Peracino [a,*], Valentina Monica [b], Luca Primo [b], Enrico Bracco [b], Salvatore Bozzaro [a]

[a] Department of Clinical and Biological Sciences, University of Torino, AOU S. Luigi, Orbassano 10043, Italy
[b] Department of Oncology, University of Turin, 10060 Candiolo, Italy

ARTICLE INFO

Keywords:
Ferric chelate reductase
Dictyostelium discoideum
Iron metabolism
Iron binding proteins
Nramp1

ABSTRACT

Iron is the most abundant transition metal in all living organisms and is essential for several cellular activities, including respiration, oxygen transport, energy production and regulation of gene expression. Iron starvation is used by professional phagocytes, from *Dictyostelium* to macrophages, as a form of defense mechanism against intracellular pathogens. Previously, we showed that *Dictyostelium* cells express the proton-driven iron transporter Nramp1 (Natural Resistance-Associated Macrophage Protein 1) and the homolog NrampB (Nramp2) in membranes of macropinosomes and phagosomes or of the contractile vacuole network, respectively. The Nramp-driven transport of iron across membranes is selective for ferrous ions. Since iron is mostly present as ferric ions in growth media and in engulfed bacteria, we have looked for proteins with ferric reductase activity. The *Dictyostelium* genome does not encode for classical STEAP (Six-Transmembrane Epithelial Antigen of Prostate) ferric reductases, but harbors three genes encoding putative ferric chelate reductase belonging to the Cytochrome b561 family containing a N terminus DOMON domain (DOpamine β-MONooxygenase N-terminal domain). We have cloned the three genes, naming them *fr1A*, *fr1B* and *fr1C*. *fr1A* and *fr1B* are mainly expressed in the vegetative stage while *fr1C* is highly expressed in the post aggregative stage. All three reductases are localized in the endoplasmic reticulum, but Fr1A is also found in endolysosomal vesicles, in the Golgi and, to a much lower degree, in the plasma membrane, whereas Fr1C is homogeneously distributed in the plasma membrane and in macropinosomal and phagosomal membranes. To gain insight in the function of the three genes we generated KO mutants, but gene disruption was successful only for two of them (*fr1A* and *fr1C*), being very likely lethal for *fr1B*. *fr1A*- shows a slight delay in the aggregation stage of development, while *fr1C*- gives rise to large multi-tipped streams during aggregation and displays a strong delay in fruiting body formation. The two single mutants display altered cell growth under conditions of ferric ions overloading and, in the ability to reduce Fe^{3+}, confirming a role of these putative ferric reductases in iron reduction and transport from endo-lysosomal vesicles to the cytosol.

1. Introduction

Iron (Fe) is an essential micronutrient for most living organisms. The transition between two oxidative states, Fe (II) and Fe (III), renders it crucial for many cellular redox processes including respiration, oxygen transport, energy production as well as other cellular processes, such as regulation of gene expression and cell death (e.g., ferroptosis) (Hirschhorn and Stockwell, 2019; Muckenthaler et al., 2017). Excess iron is also toxic for cells, as it contributes to oxidative damage, therefore cells have developed a complex network to regulate iron homeostasis. Basically, however, iron homeostasis relies on its tightly controlled uptake, considering that the only putative iron exporter, at least in higher eucaryotes, is ferroportin (Dunn et al., 2007). Depending on cell type and on the iron status (i.e., protein-conjugated, or free iron), iron uptake is mediated by two major cellular routes: heme and non-heme-dependent transport. In higher eukaryotes, the first one takes place when iron is bound, under its ferrous state, to a heme group, thus being much more bioavailable than the non-heme iron counterpart. Intestinal heme is presumably taken up via a high-affinity heme transporter, the heme-responsive gene 1 (HRG1) protein, which is also responsible for the export of the heme group from the macrophage's phagolysosome (White et al., 2013).

* Corresponding author.
E-mail address: barbara.peracino@unito.it (B. Peracino).

https://doi.org/10.1016/j.ejcb.2022.151230
Received 5 January 2022; Received in revised form 7 April 2022; Accepted 25 April 2022
Available online 28 April 2022
0171-9335/© 2022 The Authors. Published by Elsevier GmbH. This is an open access article under the CC BY-NC-ND license (http://creativecommons.org/licenses/by-nc-nd/4.0/).

Non-heme iron refers to the various forms of iron, either bound to proteins other than heme, or free inorganic iron. Non-heme iron from the diet is taken up in the apical membrane of intestinal enterocytes via the divalent metal transporter 1 (DMT1/Nramp2) and released at the basal membrane into the circulation via ferroportin 1. Plasma transferrin (Tf), the major ferric ion (Fe^{3+}) binding molecule, then delivers ferric iron in every district of the body (Gao et al., 2019). Iron-loaded Tf binds to its cognate plasma membrane receptor (TfR) and the Tf-TfR complex is then internalized via receptor-mediated endocytosis (Gao et al., 2019; Kawabata, 2019). Eventually, the low lumenal endolysosomal pH causes ferric iron dissociation from Tf, and after reduction to its ferrous form, iron is then transported from endosomes to the cytoplasm via DMT1. In the case of macrophages, the iron internalized via phagosomes is transported to the cytosol via the DMT1 homolog Nramp1. Both Nramp1 and DMT1 are proton-coupled symporters that function at acidic pH by coupling the protons flow to the transport of ferrous iron into the cells (Buracco et al., 2015b; Yanatori and Kishi, 2019). Nramp1 is highly conserved from very simple organisms to mammals, and in lower eucaryotes, such as *Dictyostelium*, where iron is taken up by phagocytosis or macropinocytosis, Nramp1 is essential for iron import to the cytoplasm (Bozzaro et al., 2013). Since both DMT1 and Nramp1 transport ferrous iron, ferric ion reduction in phago- or endo-lysosomes is crucial for iron transport to the cytoplasm. Notably, professional phagocytes, like macrophages and free-living amoebae, exploit this mechanism to iron-starve intracellular pathogenic bacteria (e.g., *Legionella or Mycobacteria*) in the phago-lysosome (Peracino et al., 2006, 2013).

The social amoeba *Dictyostelium discoideum*, has been proven an excellent model to study phagocytosis and macropinocytosis (Bozzaro et al., 2019, 2008; Kay, 2021; Williams and Kay, 2018), and to ascertain the role of divalent metals during growth and resistance to intracellular pathogenic bacteria (Bozzaro et al., 2013, 2008; Hanna et al., 2021; Steinert, 2011). In *Dictyostelium* cells iron uptake occurs through macropinocytosis or phagocytosis of living particles, such as bacteria or yeasts (Peracino et al., 2013). Besides that, the exact route followed by iron once internalized has been extensively characterized. The iron entrapped within the vesicles is released into the cytoplasm by the proton-driven transport mediated by Nramp1 (Bozzaro et al., 2013; Buracco et al., 2018, 2015b). The *Dictyostelium* genome does not harbor a classical ferritin for binding "free" cytosolic iron, though a distantly related bacterial ferritin is encoded. However, in the membrane of the contractile vacuole network is located a homolog of Nramp1, NrampB, as well as the same V-H^+ ATPase, responsible for acidification of phagosomes and macropinososmes, thus allowing a proton-driven transport of excessive "free" iron in the vacuole (Peracino et al., 2013). Evidence has been provided that the contractile vacuole acts as a sort of store or sink for divalent metals, such as iron, zinc or calcium, which can be expelled by fusion of the contractile vacuole with the plasma membrane or, alternatively, re-transported to the cytosol when needed via divalent metal transporters (Barisch et al., 2018; Bozzaro et al., 2013; Buracco et al., 2018; Parkinson et al., 2014; Peracino et al., 2013).

The Nramp1-mediated iron transport from phagolysosomes to the cytosol foresees a ferric reductase coupled to Nramp proteins, but classical STEAP ferric reductases as in mammals (Ohgami et al., 2006) are not encoded in the *Dictyostelium* genome. Here we report the identification, isolation, and functional characterization of three novel *Dictyostelium* ferric reductase encoding genes. Their structural features are shared with members of the cytochrome b561 family. Homologous recombination-mediated genes deletion, in-vivo intracellular localization of the corresponding encoded proteins and proof of ferric iron reduction suggest that they contribute to regulate *Dictyostelium* iron homeostasis.

2. Materials and methods

2.1. Cell and bacterial strains and culture methods

The following *Dictyostelium discoideum* clones were used throughout the study: parental strain (AX2), overexpressing strains AX2:Fr1A-GFP, AX2:Fr1B-mRFPmars, AX2:Fr1C-GFP AX2:Nramp1-GFP, AX2:NrampB-GFP (Peracino et al., 2013, 2006), AX2:Calnexin-GFP (Müller-Taubenberger et al., 2001) as well as single or double KO mutants in *fr1A* and *fr1C*.

All strains were cultured either in axenic (Ashworth and Watts, 1970) or minimal medium (Franke and Kessin, 1977) at 23◦C under shaking at 150 rpm in a climatic cabinet equipped with gyratory shakers (Kuehner, Bielefeld, Switzerland) (Peracino et al., 2006). The knockout mutant strains were cultured in presence of 10 μg/ml of blasticidin, whereas the clones expressing GFP-tagged proteins were cultured in the presence of 10 or 20 μg/ml G418.

For growth and development on nutrient agar, cells were mixed with *Escherichia coli* B/2, plated on nutrient agar plates, and incubated at 23 °C (Sultana et al., 2005). Growth and development were observed with a stereomicroscope and pictures were taken with a webcam MikrOcular 3,0 MP (Bresser 59-13200) connected to a PC computer.

2.2. Cells development on non-nutrient agar plates

For synchronizing development, exponentially growing cells were harvested from culture medium, washed twice in 0.017 M Soerensen Na/K phosphate buffer (pH 6.0) and resuspended in the same buffer at a concentration of 1 × 107 per ml. Aliquots of 0.05 ml were plated on Soerensen phosphate agar plates at a density of ~3 × 105 cells per cm^2, and incubated at 23◦C (Sillo et al., 2008).

2.3. Ferric reductase assay

Mid-log axenically growing cells were harvested and washed three times in Soerensen phosphate buffer. A total of 5 × 10^6 cells were resuspended in the assay buffer (5 mM MOPS, 25 mM MES, 5.4 mM KCl, 5 mM glucose, 140 mM NaCl, 1.8 mM $CaCl_2$, 0,8 mM $MgCl_{2)}$ supplemented with 0.1 mM Fe (III)- nitrilotriacetic acid –NTA (Sigma cat. N. NO128) and 0.2 mM 3-(2-pyridyl)− 5,6-diphenyl-1,2,4-triazine-4′,4′′-disulfonic acid sodium salt (Ferrozine, Sigma), plated in a 24 well plate and incubated in the dark for 90 min at 23 °C. At the end of the incubation, the plate was centrifuged 5 min at 450 g and the iron reduction recorded by measuring the supernatant absorbance at 562 nm (Wyman et al., 2008). Standard curves were generated to convert the absorbance value into μg of Fe^{2+} and values were then normalized to 10^6 cells.

2.4. Sequence analysis

Protein and gene sequences were obtained using a basic search tool Blast at the DictyBase site (http://dictybase.org/). Protein homologs were identified by using Blast at the NCBI site (http://www.ncbi.nlm.nih. gov/BLAST/). Multiple sequence alignment was performed using ClustalW. Putative transmembrane regions were identified by using Protter tool (http://wlab.ethz.ch/protter/).).

Phylogenetic analysis was performed using the MacVector software.

2.5. Gene cloning, plasmid construction and Dictyostelium cells transformation

The *fr1* genes (*fr1A*/DDB_G0283271; *fr1B*/DDB_G0279437 and *fr1C*/DDB_G0270284) were PCR amplified using AX2 genomic DNA as template using gene specific primers (Table 1). The PCR products were cloned into the pGEM-TEasy vector (Promega, Madison, WI, USA).

For fusion with GFP or mRFPmars, the *fr1A* and *fr1C* genomic sequences were amplified by using gene specific primers harboring *Eco*RI

Table 1
Sequences of gene specific primers used for cloning Dd Ferric chelate reductases.

FW DDB_G0283271	5′-CAACACCCACAACATTTAAAAATTC-3′
RW DDB_G0283271	5′-CCATAGAATCTTTTATGAATTTCTAAAGC-3′
FW DDB_G0279437	5′-AAATGATAAAATCGATTGTGTTTTTAAGC-3′
RW DDB_G0279437	5′-CCTTATTTTCACATGATGTCATTTTTTT-3′
FW DDB_G0270284	5′-AAAAATGAAAAATAATTATTCATTGC-3′
RW DDB_G0270284	5′−3′AAAATTAAAAATTAATTATTTATATTTATGG

or *Bam*HI sites at each end. The amplicons were then inserted into the *Eco*RI site of the pDEX-GFPC vector (Westphal et al., 1997) or in *Bam*H1 site of 389-2pDEXR (H)-mRFPmarsC vector (Fischer et al., 2004). Cell transformation was carried-out by electroporation (Pang et al., 1999) and transformants were selected in axenic medium containing G418 at final concentration of 10 μg/ml.

2.6. Construction of single Fr1A, Fr1C and double Fr1C/A knockout mutants

The blasticidin cassette was excised from the pLPBLP (floxed Bsr) vector (Faix et al., 2004) with *Sma*I and blunt-end cloned either in the EcorV site of a fragment of ~1200 bp of the *fr1A* gene; or alternatively in the single *Sma*I site, generated by site-directed mutagenesis (QuickChange Agilent cat. n. 200519-4) and localized at around 150 bp downstream of the *fr1C* intron. These fragments carrying the selectable markers were used to transfect the parental *Dictyostelium* AX2 cells and generate the single knockout mutant strains. The transformed cell population was then cloned in 96-well plates and grown in the presence of 10 μg/ml of blasticidin. Resistant clones were screened by PCR using locus specific primers (Table 2; Fig. 3A; Supplementary Table 1).

After a phenotypic analysis of three independent clones, one *fr1C* KO clone was treated with pDEX-NLS-cre to transiently express the CRE recombinase and remove the blasticidin cassette (Kimmel and Faix, 2006). Afterwards, the cells were further transformed to disrupt the *fr1A* gene. After blasticidin selection, putative double knockouts clones were screened by PCR.

2.7. Gene expression analysis by quantitative PCR

Total RNA was extracted with TRIzol (Invitrogen, Carlsbad, CA, USA) from cells at different developmental time points and analyzed by quantitative RT-PCR (qRT-PCR). Total RNA was treated with DNase and retrotranscribed with random hexamer primers and Multiscribe Reverse transcriptase (High-Capacity cDNA Archive Kit; Applied Biosystems, Foster City, CA). Expression levels of *fr1A*, *fr1B*, *fr1C* and reference *RNLA* were assessed with SYBR technology. Primer sequences are listed below (Table 3).

Melting curve analysis and efficiency evaluation were performed for all the amplicons. Baselines and thresholds for Ct calculation were set up manually with the ABI Prism SDS 2.1 software.

Table 2
KO screening strategy: Dd Ferric chelate reductases knock-out PCR screening primers.

F1 primers (FW)	
Dd fr1A	5′-TACTACTCAAATTCTAATATTACTTTCG-3′
Dd fr1C	5′-GGTGATAGAGATTTATTTGTGG-3′
R2 primers (RW)	
Dd fr1A	5′-TTGATTGAATGACAATGTGGAG-3′
Dd fr1C	5′-GCTATTAAATAAGTTAATCTTGCC-3′
R3 primers (RW)	
Dd fr1A	5′-GAGAAGTTACTTTGCTTTGAGCCAC-3′
Dd fr1C	5′-GGCAGCTGAGAATATTGTA-3′
F4 primer (FW)	
BSD_out	5′- CATTCCACTCAAATATACCCG-3′

Table 3
Dd Ferric chelate reductases gene expression primers.

Dd fr1A FW	5′-TCAACCGCTTTGGCATTCA-3′
Dd fr1A RW	5′- ACGCCATCGTGCTTAACCA-3′
Dd fr1B FW	5′- GATAATTCATTTGGCTTCCATGGT-3′
Dd fr1B RW	5′- CCGGTGGCAAGATTCACTGT-3′
Dd fr1C FW	5′- TGTGGATGGAAGAATGACAACTTT-3′
Dd fr1C RW	5′- TTGACCGTGATATGTTAAATTTTGG-3′
RNLA FW	5′- GCACCTCGATTCGGCTTAAC-3′
RNLA RW	5′- CACCCCAACCCTTGGAAACT-3′

2.8. In vivo microscopy, fluorescence imaging and immunofluorescence

To label ferrous iron containing vesicles, living cells were incubated with 5 μM FeRhoNox™-1 (Goryo chemical) and 0.1 or 0.2 mM $FeCl_3$ in LoFlo medium (Formedium™) for 90 min in a 24 well glass bottom plate (Ibidi GmbH, Planegg/Martinsried, Germany) and incubated at 23 °C.

To label endocytic and phagocytic vesicles, GFP- or mRFPmars-Fr1 expressing cells were incubated with 1 mg/ml TRITC-dextran or with inactivated yeast particles. For immuno-labeling, cells were fixed with cold methanol, incubated with antibodies against either the A subunit of the V-H^+-ATPase (Fok et al., 1993), comitin (Weiner et al., 1993) or PDI (Monnat et al., 1997) as described (Peracino et al., 1998). Secondary fluorescent antibody AlexaFluor488 or AlexaFluor555 (Thermo Fisher Scientific) were used. Nuclei were labeled with DAPI (Sigma cat. n. D8417).

Confocal series images were taken on an inverted Zeiss LSM800 with AiryScan (Carl Zeiss, Inc., Oberkochen, Germany) equipped with a Plan-Apochromat 63x/1.40 DIC Oil immersion objective. Phase contrast pictures were recorded simultaneously with 517 nm emission channel.

3. Results

3.1. Identification, isolation, structural characterization, and developmental gene expression of the Dictyostelium ferric reductase family members

To identify *Dictyostelium* ferrireductase encoding genes, BLAST searches against the *Dictyostelium* genome database using the amino acid sequence of the human ferric reductase DCYTB domain (Tsubaki et al., 2005) were performed, since the human DCYTB is the reductase associated to DMT1 in mammalian cells and responsible for reduction of iron transported across the membrane by DMT1. Three putative family members, named *fr1A* (DDB_G0283271), *fr1B* (DDB_G0279437) and *fr1C* (DDB_G0270284) were identified based on their sequence similarity to DCYTB ferric reductases, displaying a predicted theoretical molecular mass of approximately 40 kDa. Though the three genes are expressed throughout the whole *Dictyostelium* life cycle, the *fr1A* and *fr1B are* expressed at their highest level during the vegetative stage, whereas the *fr1C* is principally expressed at the post-aggregative phase (Fig. 1A). Consistently, these data are congruent with those from the transcriptomic profile of developmental time course on filter, of AX4 *Dictyostelium* cells, filed at the dictyExpress (https://dictyexpress.research.bcm.edu) (Fig. 1B) (Rosengarten et al., 2015; Stajdohar et al., 2017).

Protein sequence analysis showed that Fr1A shares 33% identity with Fr1B and 27% with Fr1C, while Fr1B shares 40% identity with Fr1C, and the similarity between the three proteins varies from 47% (Fr1C vs. Fr1A) to 60% (Fr1B vs. Fr1C). (Fig. 2A).

The sequence analysis of the three *Dictyostelium* putative ferric reductases displayed a few peculiar common features: (a) five hypothetical transmembrane domains; (b) four conserved histidine (His) residues localized between the first and the fourth transmembrane domain, proposed to act as two heme ligands in mammalian ferric reductase of the Dcytb family (Asard et al., 2013), and (c) a predicted N-terminus DOMON (dopamine β-monooxygenase) domain that should provide

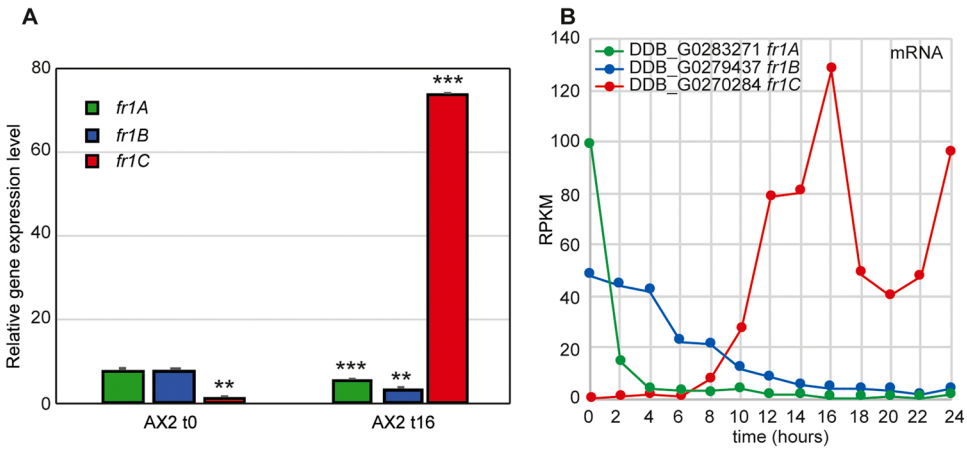

Fig. 1. fr1A, fr1B and fr1C gene expression at vegetative and post aggregative stage. (A) Axenically growing AX2 cells were washed free of medium and plated on Soerensen phosphate agar. Cells were collected at t0 (vegetative-) and at t16 (mound-stage) from agar plates. RNA was extracted and amplified with appropriate primers as described in Materials and Methods. Fold changes at each time point are relative to the constitutively expressed RNLA gene as internal control. Mean values (+ Standard Deviation -SD-) of at least two independent experiments are shown. Statistics was assessed by mean of a non-parametric t-test (asterisks denote significant differences ** $P < 0.01$ *** $P < 0.001$). (B) *fr1s* gene expression time course assessed by transcriptome profiling time course of AX4 cells developed on filter (https://dictyexpress.research.bcm.edu).

electrons for the CYB561core. Notably, all three proteins contain a N-terminal signal peptide (Fig. 2B). The predicted *Dictyostelium* Fr1s protein structure is common to some plant homologs and to the mammalian FRRS1 proteins, including mouse SDR2 (Vargas et al., 2003). The predicted *Dictyostelium* Fr1s protein structure is shared with some plant homologs and with the mammalian Fr1 proteins, including mouse SDR2 (Vargas et al., 2003). The phylogeny analysis of the Dd Fr1 proteins locates them closer to mouse and *Drosophila,* rather than to plant and the human *CYBR* members (Fig. 2C).

3.2. Effects of fr1A and fr1C gene disruption by homologous recombination

To investigate the functional role of the three *Dictyostelium* ferric chelate reductases, we attempted to generate KO mutants by homologous recombination (Fig. 3A).

Gene disruption was fruitful for two of the three *Dd fr1s* genes. *Dictyostelium fr1A* and *fr1C* null mutants were successfully generated, whereas we failed to attain a *fr1B* null strain, albeit we screened approximately 450 blasticidin-resistant clones. This result is strongly suggestive of *fr1B* to be an essential gene.

Noteworthy, we also generated a double *fr1C/A* KO mutant.

We tested the relative expression of the three genes in the KO mutants, to assess whether gene disruption affected the expression of the intact genes. In cells growing in axenic medium, the *fr1B* mRNA accumulation increased robustly in the *fr1A* and *fr1C* single KO strains, and to a higher extent in the double *fr1C/A* mutant (Fig. 3B) suggesting that cells tend to overcome the absence of either one or both the disrupted genes by enhancing the expression of *fr1B*. The *fr1A* mRNA expression increased also in the *fr1C*- mutant, but to a much lower extent than *fr1B* (Fig. 3B).

We assayed the growth rate of KO mutants on a lawn of *E. coli* B/2. The growth rate on bacterial lawn was reduced for all mutants, with the double mutant displaying a greater reduction when compared to the *fr1A* and to *fr1C null mutants* (Fig. 4A). These observations suggest that Fr1A and Fr1C act as positive regulators when cells graze on a bacteria lawn.

Conversely, when cells were cultured in axenic medium, we did not detect any significant difference in the growth rate, with the only exception of *fr1A* null mutant, which displayed a very modest, though statistically significative, increase in the doubling time. Expressing Fr1A-GFP in the mutant background restored the normal value (Fig. 4B).

All mutants were able to complete development on non-nutrient agar plates, but in *fr1C*- development was delayed of approximately 6 h, taking more than 30 h to form mature fruiting bodies (Table 4).

In addition, deleting *fr1C* resulted in formation of very large, partially multi- tipped aggregating streams, which underwent fragmentation, before forming fruiting bodies (Fig. 5A). Interestingly, in the double mutant *fr1C/A*– development was like the parental AX2 (Table 4 and Fig. 5A). Expressing under a constitutive promoter Fr1C-GFP in the *fr1C*- mutant did not rescue the aggregation phenotype but resulted in further delay of development (Table 4 and Fig. 5B). We therefore constitutively expressed Fr1C-GFP also in the AX2 background. Fr1C-GFP induced large and multi-tipped aggregates and delayed development (Fig. 5B and Table 4). Constitutive expression of Fr1A-GFP in the AX2 background did not affect aggregation and formation of tight mounds, though of a smaller size, but later development was strongly delayed with many mounds still present at t36 together with some fruiting bodies (Fig. 5B and Table 4). Remarkably, in the *fr1A*- mutant, Fr1A-GFP expression did not affect the timing of early development and aggregation, but many mounds flattened and underwent spiral and whirl movements for several hours before forming fruiting bodies with a delay of about 8 h compared to *fr1A*- (Fig. 5B and Table 4).

3.3. Fr1A and 1B are predominantly confined to ER membrane while Fr1C is localized mainly in the plasma membrane

To assess the "in-vivo" intracellular localization of the three putative DdFR1s, we generated chimeric proteins by fusing GFP, or mRFPmars, at their C-terminus.

In vivo cellular analysis of cells expressing the ferric reductases fused with fluorescent tags revealed that all three proteins were predominantly confined in the membrane of several intracellular vesicles. Furthermore, immunolabeling with a specific marker of the Endoplasmic Reticulum (ER) lumen, namely an antibody against the Protein Disulfide Isomerase (PDI) (Monnat et al., 1997), showed co-localization, indicating that the three Dd FR1s reside in the ER (Fig. 6). Immunostaining with antibodies against the A subunit of the V-H^+-ATPase (vatA), which labels membranes of acidic vesicles and the contractive vacuole network (Fok et al., 1993) or against comitin, which labels the Golgi apparatus (Weiner et al., 1993) were also carried-out. Interestingly, the co-localization of these markers with Fr1s revealed some differences in the distribution of the three proteins. In addition to the ER, Fr1A was found in the membranes of some endocytic vesicles as wells as in Golgi vesicles (Fig. 6A). Fr1B, instead, co-localizes almost exclusively with PDI, thus selectively in the ER (Fig. 6B), whereas Fr1C was homogenously distributed at the level of the plasma membrane, in addition to some ER, endocytic and Golgi vesicles (Fig. 6C). Fr1A was also found in the plasma membrane (Fig. 7A), but not as sharply as Fr1C.

Since Fr1A and Fr1C colocalize partially with acidic endocytic vesicles, we attempted to assess whether these two reductases might be recruited to macropinosomal or phagosomal vesicles, by incubating cells expressing the chimeric proteins with TRITC-Dextran or inactivated yeast particles. FR1A was recruited within few seconds after TRITC-

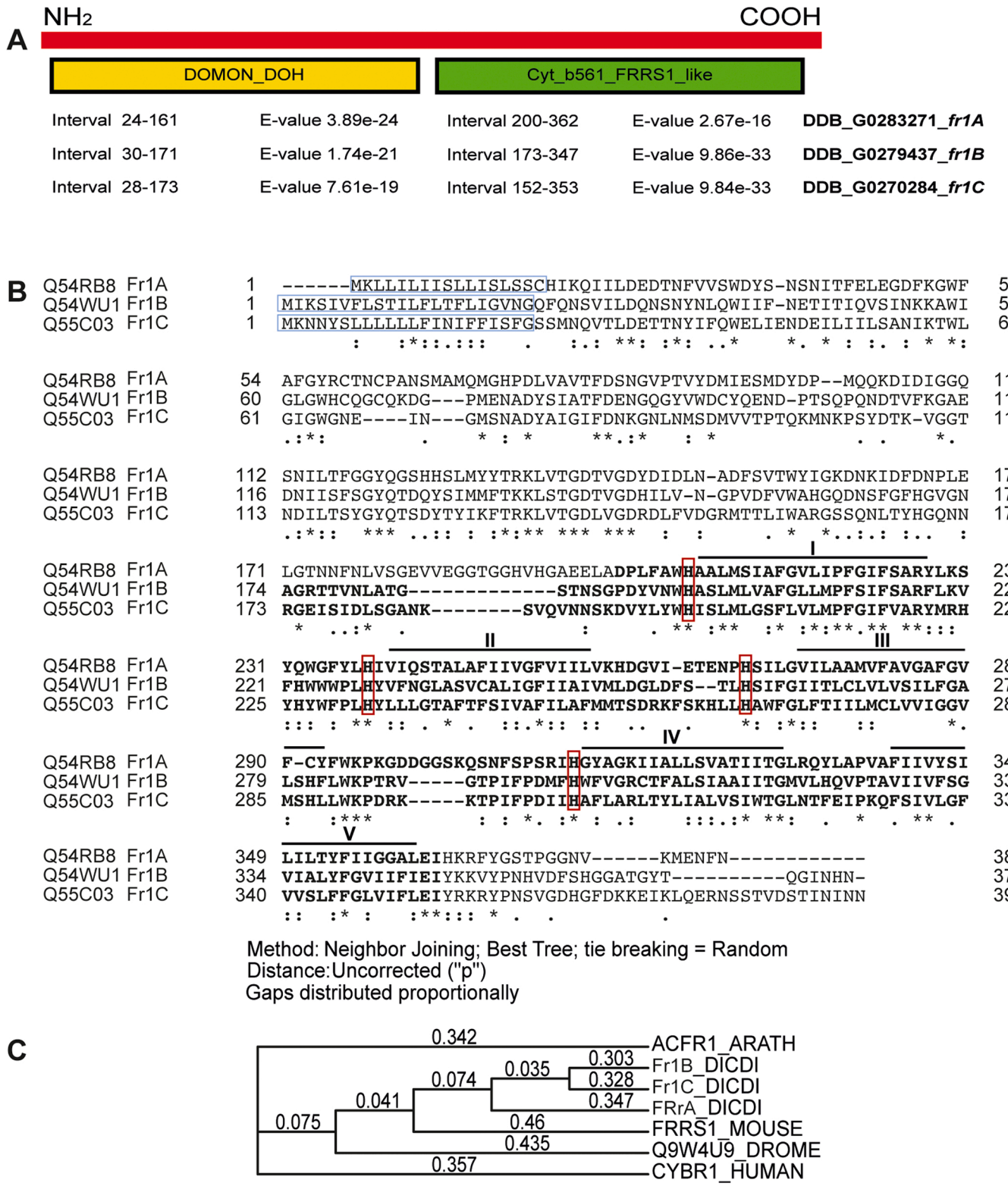

Fig. 2. *Dictyostelium discoideum* Ferric chelate reductases Fr1A Fr1B and Fr1C. (A) Graphical representation of conserved protein domains presents in Dd Fr1 proteins. (https://www.ncbi.nlm.nih.gov/Structure/cdd; Blastp program at https://blast.ncbi.nlm.nih.gov) e-value is the parameter describing the number of hits one can "expect" to see by chance when searching a database. (B) All sequences are aligned using Clustal Ω by UniProt web site (https://www.uniprot.org/). Identical residues are marked by asterisks and residues with strongly or weakly similar properties with double and single points, respectively. Blue boxes indicate signal peptide sequence; Red boxes indicate the four highly conserved histidine residues for putative heme binding domain; numbered black lines indicate the putative trans-membrane domains; amino acid sequences in gray indicate the DOMON domain and amino acid sequences in bold indicate CYB561 domain. (C) Phylogenetic relationship of *Dictyostelium discoideum* Fr1s protein and other CYB561 and DOMON domain containing Cyb561 proteins. Sequences were compared to similar sequences using the MacVector software and performing multiple sequence alignment with the ClustalW program (Blosum matrix). The evolutionary distance was inferred using the neighbor joining method. The percentage of replicate trees in which the associated taxa clustered together in the bootstrap test (1000 replicates) are shown next to the branches. UniProt accession number and identifiers are shown.

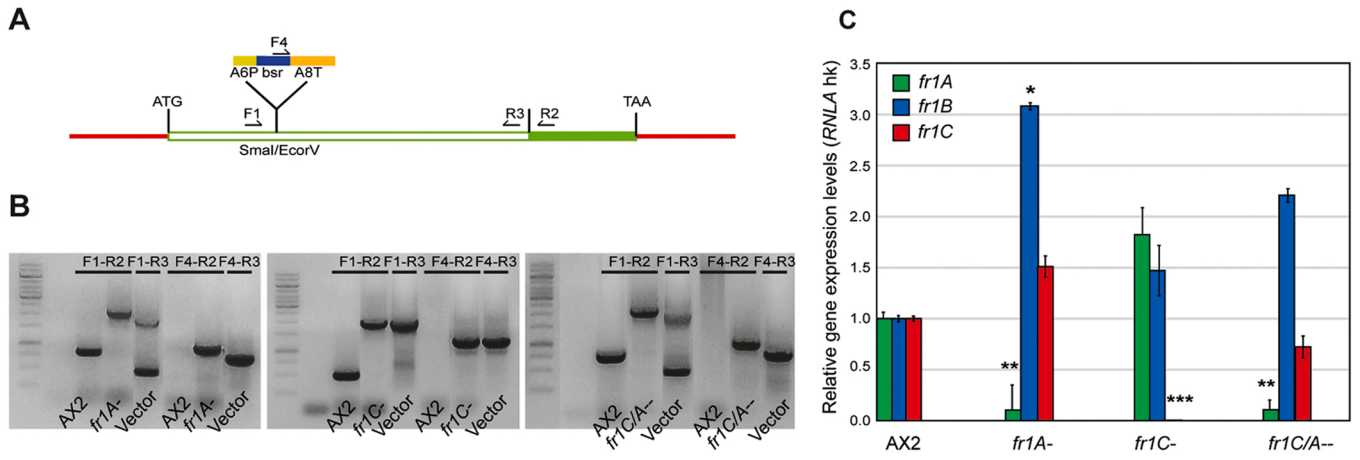

Fig. 3. Generation of fr1 mutant clones. (A-B): Schematic procedure for *fr1A, fr1C* and *fr1C/A–* gene disruption and evidence by PCR of generated mutant clones. A *bsr* cassette flanked with *loxP* recombination sites, one of which contained stop codons in all six reading frames (Faix et al., 2004), was inserted in the *genes* in *SmaI* site generated by site mutagenesis or in EcorV (see materials and methods). The linearized plasmid was electroporated in cells and clones were analyzed by PCR by using the primers (Table 1) in the combination shown in the schematic graphic. In (B) on the left of each gel at bottom is shown the recombination by the shift of the band; on the right is shown the locus *interruption* of the clones. (C) FR1s' mRNA expression in *fr1A-, fr1C-* and *fr1C/A–* mutant clones. RNA was extracted from vegetative cells in exponential phase and analyzed by qPCR to compare the relative expression of the three *fr1s* (*fr1A, fr1B and fr1C*) in parental cells (AX2) versus the KO mutants (*fr1A-; fr1C-* and *fr1C/A–*). The expression values of each gene in the mutants were normalized to the corresponding RNA levels in AX2 and plotted as mean (+ SD). Statistics was assessed by mean of a non-parametric t-test (asterisks denote significant differences * $p < 0.05$; ** $P < 0.01$ *** $P < 0.001$).

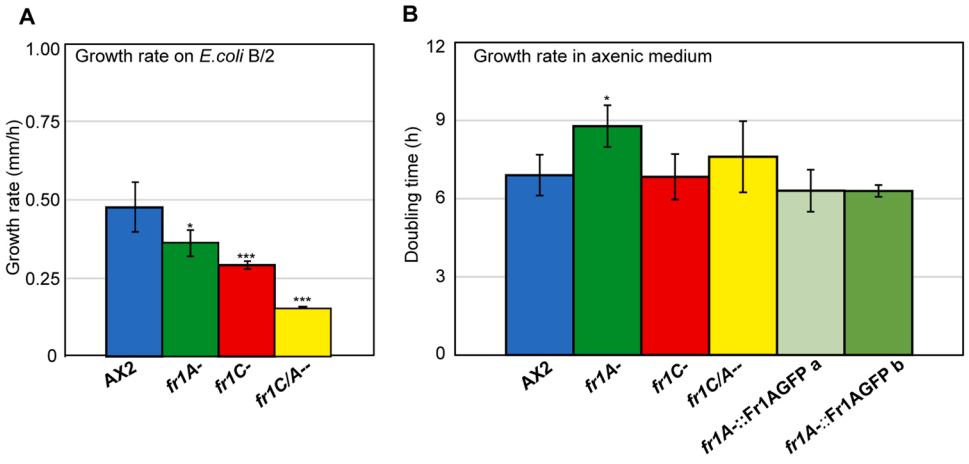

Fig. 4. Effects of single or double gene disruption on cell growth. (A) Parental strain and cells of KOs were plated on *E. coli* B/2 lawn on Normal agar plates. Growth rate was measured by quantifying the rate of plaque expansion. The mean and the standard deviation (SD) values of three independent experiments are shown in the graph. (B) Parental strain and cells of KOs were grown in axenic medium, and the growth rate was measured by calculating the doubling time expressed in hours during the exponential phase. The mean values and the standard deviation (SD) of 10 independent experiments. Statistics was assessed by mean of a non-parametric t-test (asterisks denote significant differences * $p < 0.05$; *** $P < 0.001$).

Table 4
Developmental time (hours) of *Dd fr1* knock out mutants.

Strain	Aggregation	Tip mounds	First-finger	Fruiting bodies
AX2	t6 + /– 1	t12 + /– 1	t16 + /– 1	t24 + /– 1
fr1A-	t6,5 + /– 1	t12 + /– 1	t16 + /– 1	t24 + /– 2
fr1C-	t12 + /– 2	t18 + /– 2	t22 + /– 1	t34 + /– 3
fr1C/A–	t7 + /– 2	t12 + /– 1	t16 + /– 1	t24 + /– 2
AX2:Fr1AGFP	t6 + /– 1	t12 + /– 1	ND	t36 + /– 4
fr1A-:Fr1AGFP	t16 + /– 2	t24 + /– 2	t34 + /– 3	t40 + /– 2
AX2:Fr1CGFP	t14 + /– 2	t16 + /– 2	t24 + /– 2	t46 + /– 2
fr1C-:Fr1CGFP	t16 + /– 2	t24 + /– 2	t34 + /– 3	t40 + /– 2

Dextran engulfment in macropinosomes with a kinetics like that of the recruitment of the V-H^+-ATPase (Clarke et al., 2010; Peracino et al., 2006) (Fig. 7).

Co-incubation of Fr1CGFP expressing cells with TRITC-labeled heat-treated yeast particles showed clear recruitment of the protein in the phagocytic cup and in the engulfed phagosome (Fig. 7C). Fr1C persisted on the membrane enclosing the internalized yeast particle until its extrusion from the cell (Supplementary Fig. 1). Tiny vesicles coated with Fr1B appear to be also recruited around the engulfed phagosome (Fig. 7B), consistent with the observation of a direct link between the ER and phagosomal membranes during phagocytosis (Müller-Taubenberger et al., 2001).

3.4. Differential FERhonox-1 labeling of intracellular vesicles and evidence for Dd FR1 ferric reductase activity

To appraise whether Dd Fr1s containing vesicles are enriched in ferrous iron we incubated cells with the activatable fluorescent probe FeRhonox-1. FeRhonox-1 specifically and irreversibly binds to labile Fe^{2+} ions resulting in red or orange fluorescence (Hirayama et al., 2013; Hirayama and Nagasawa, 2017).

Dictyostelium cells expressing Nramp1-GFP; NrampB-GFP; Calnexin-GFP; Fr1A-GFP and Fr1C-GFP, were incubated for two hours or overnight with 5 μM FeRhonox-1 in presence of 100 μM $FeCl_3$ and then observed with the confocal microscope. Vesicles containing fluorescent FeRhonox-1 were negative for the following intracellular markers: NrampB, Calnexin or Fr1C. On the contrary, Nramp1-GFP and, to a quite broad extent, Fr1A and V-H^+-ATPase containing vesicles were positive for Ferhonox-1 fluorescence (Fig. 8), indicating the luminal presence of Fe^{2+} in endo-lysosomal vesicles.

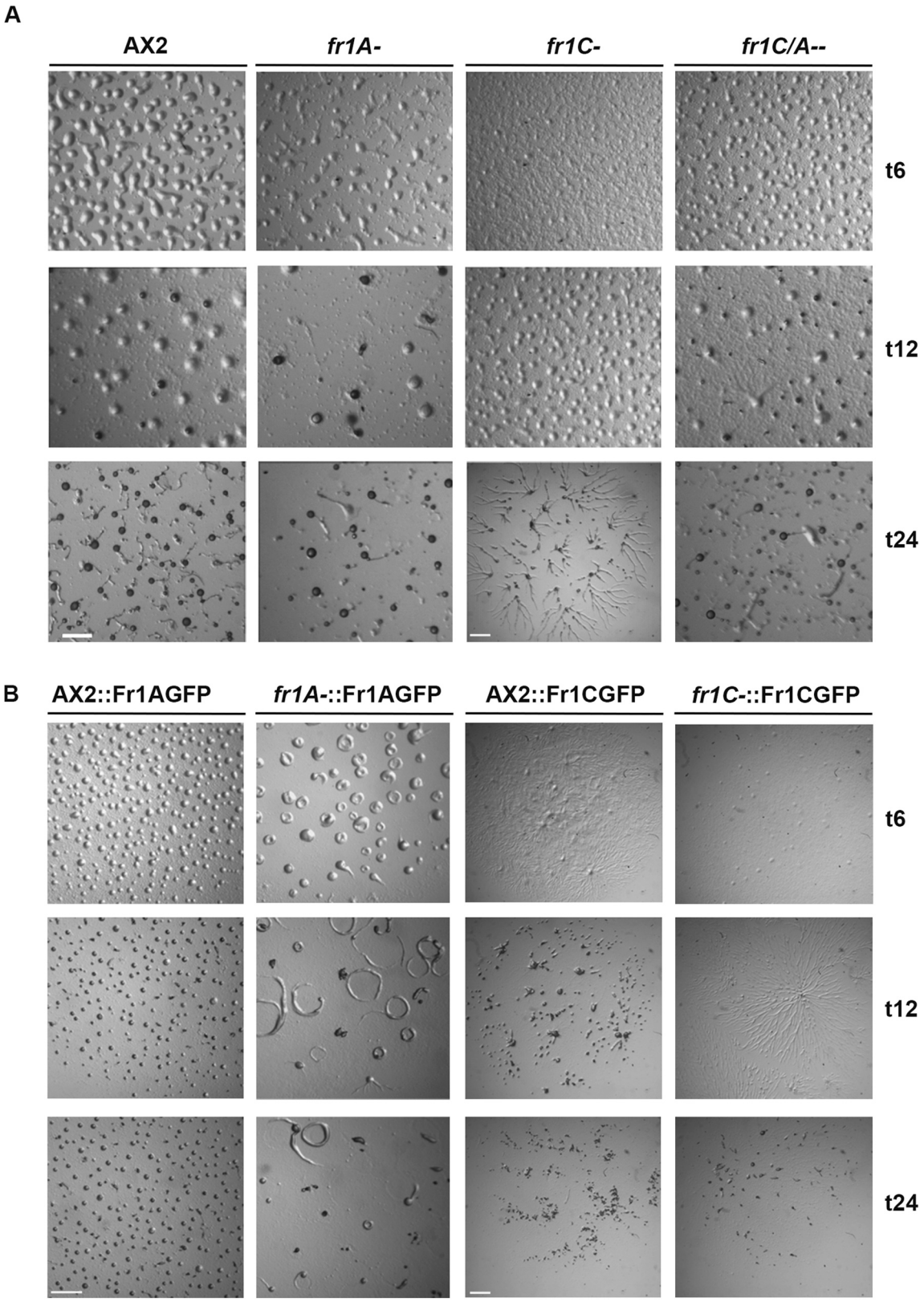

Fig. 5. Effects of single or double gene disruption on development. Starving cells of parental strain and mutants or cells overexpressing the GFP-fused proteins were plated on non-nutrient Soerensen phosphate agar and development was monitored over time with a stereomicroscope. A) In contrast to AX2 and *fr1A*-, development is delayed of several hours in the *frs1C*- mutant, with fruiting bodies formed at around 34 h. In addition, during aggregation, the mutant forms very large streams, which undergo fragmentation (see t24). Remarkably, in the *frs1A/C*– mutant, this phenotype is rescued. In AX2 expressing the Fr1C-GFP protein a phenotype resembling *fr1C*- is generated. B) Expression of Fr1A-GFP in AX2 results in a delay in postaggregative development, whereas its expression in the *fr1A*- mutant induces mound flattening and spiral and whirl movements up to 16–24 h with fruiting bodies formed by 36 h (one clone out of two is shown). Scale bars: 1 mm.

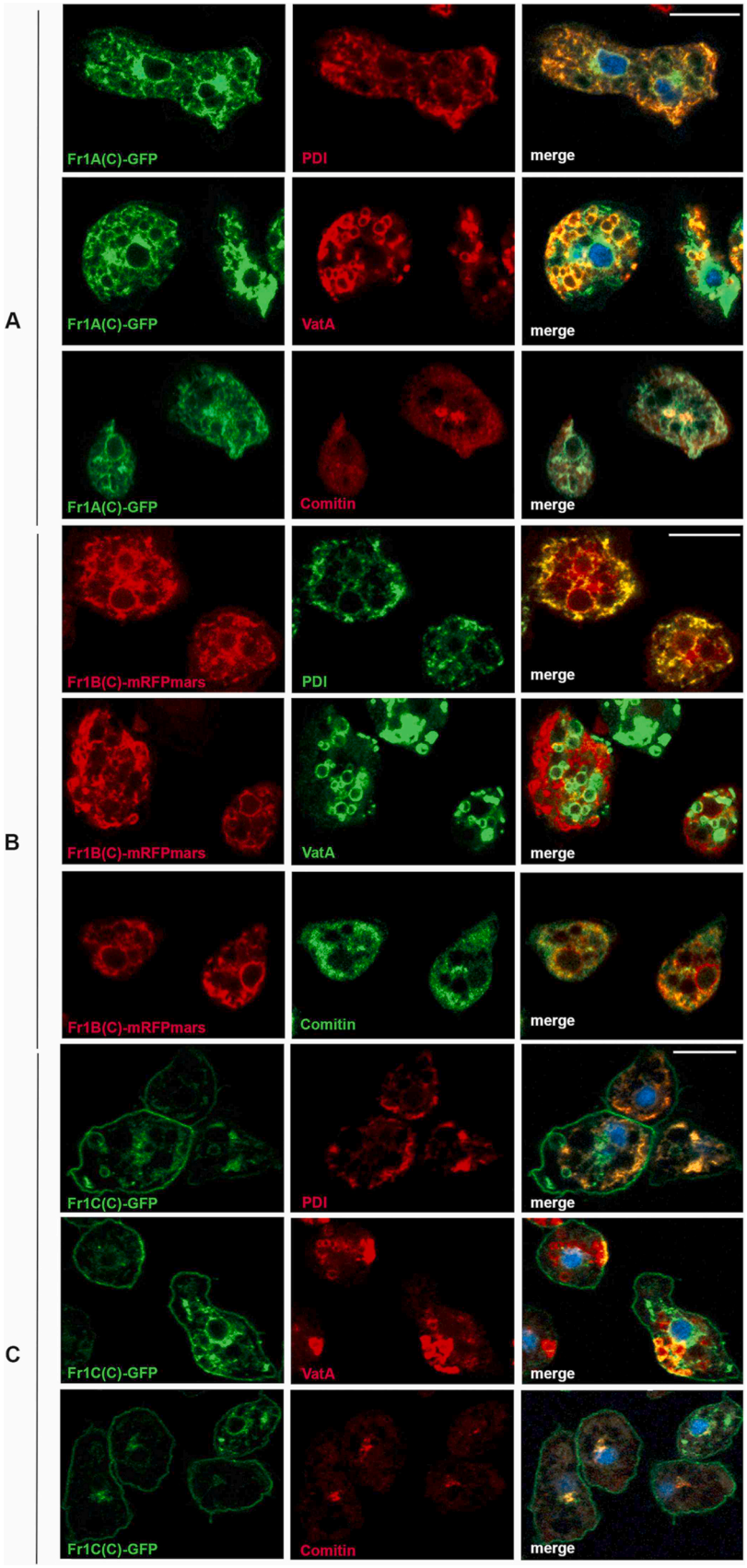

Fig. 6. Intracellular localization of Fr1A, Fr1B and Fr1C tagged with GFP or mFRPmars. Cells expressing Fr1AGFP, Fr1BmRFPmars or Fr1CGFP were fixed with ice cold methanol and labeled with antibodies against PDI, V-H+ ATPase or Comitin to locate, respectively, the endoplasmic reticulum, endolysosomal vesicles or the Golgi apparatus. (A) Fr1A is found in membranes of the endoplasmic reticulum, endolysosomal and Golgi vesicles. (B) Fr1B is mainly localized on ER membranes. (C) Fr1C decorates both the plasma membrane and in Golgi vesicles. Bar: 5 μm.

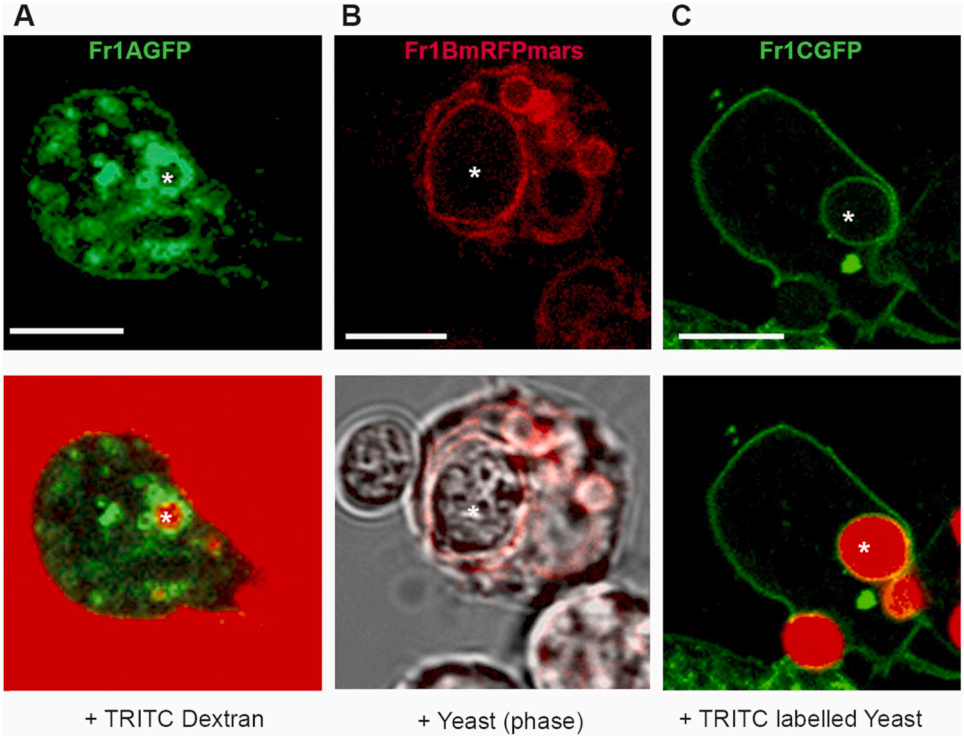

Fig. 7. Recruitment of Fr1A, Fr1B or Fr1C tagged with GFP or mFRPmars on the membrane of macropinosomes or phagosomes. Cells expressing Fr1AGFP; Fr1BmRFPmars and Fr1CGFP, respectively, were incubated with TRITC Dextran, that is taken up by macropinocytosis (A), unlabeled heat-inactivated (B) or TRITC-labeled heat-inactivated yeast particles (C) that are internalized by phagocytosis. In all three examples, the internalized dextran fluid or yeast particles are decorated with the GFP- or mRFPmars-tagged proteins. In (B) the unlabeled yeast particle is marked by an asterisk. Bar: 5 μm.

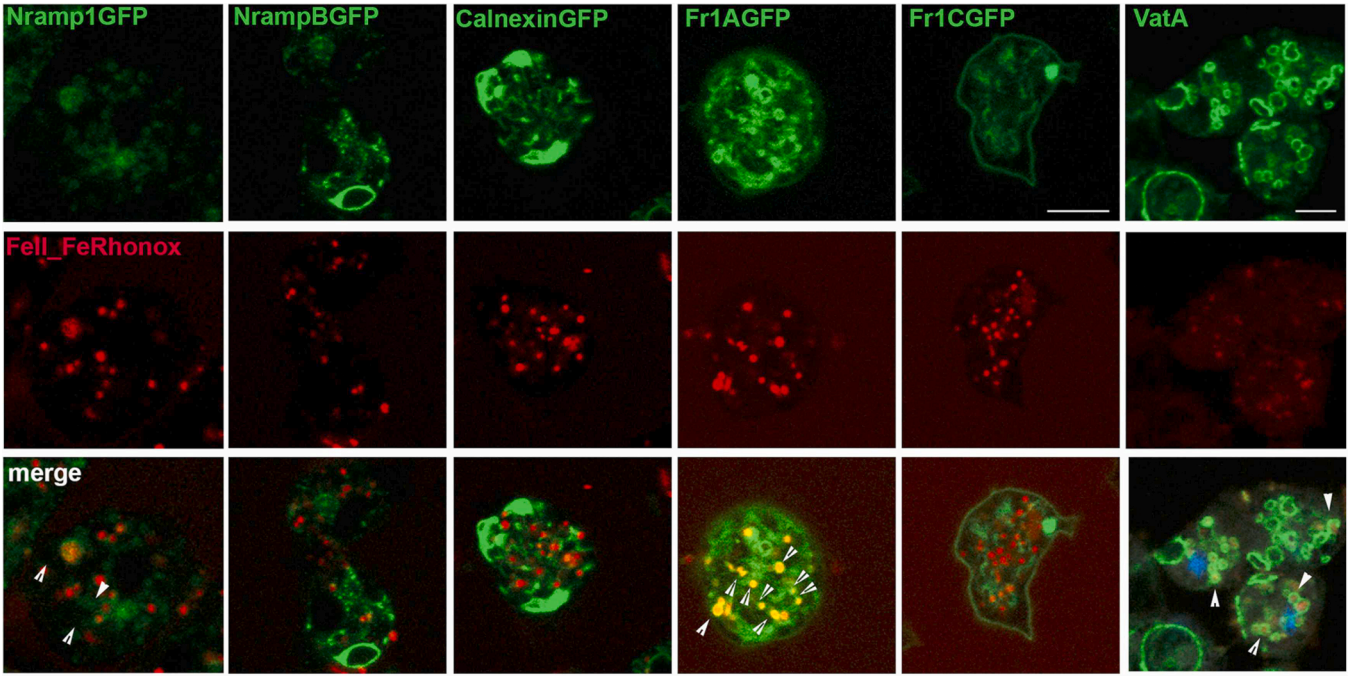

Fig. 8. Characterization of Fe^{2+} containing vesicles. Cells expressing Nramp1-GFP; NrampB-GFP; Calnexin-GFP; Fr1A-GFP; Fr1C-GFP or labeled with antibodies against the subunit A (vatA) of the V-H^+-ATPase were incubated with FeRhonox™-1 for at least two hours and observed under confocal microscopy. Arrows indicate colocalization of ferrous iron containing vesicles with the indicated proteins. *Bar:* 5 μm.

In addition, we aimed to functionally characterize the Dd Fr1s for their ability to reduce iron by measuring Fe^{2+} formation in Fr1C overexpressing strains through a colorimetric assay based on Ferrozine. The Ferrozine assay measures the extracellular accumulation of Fe^{2+}, therefore it can be used to detect ferric reductase activity located on the plasma membrane. Cells overexpressing Fr1C showed a robust increase in Fe^{3+} reduction activity (Fig. 9A), thus confirming that the DdFr1s are ferric reductase enzymes.

These results prompted us to examine the ability of the KO clones to grow under iron overload conditions. Consistently with the ability to reduce Fe^{3+}, the single *fr1A* and the double *fr1A/C* null mutants were unable to grow when minimal medium was supplemented with $FeCl_3$, whereas the *fr1C* null mutant grew almost as well as the parental AX2 strain (Fig. 9B). Thus, the defective growth in the double mutant

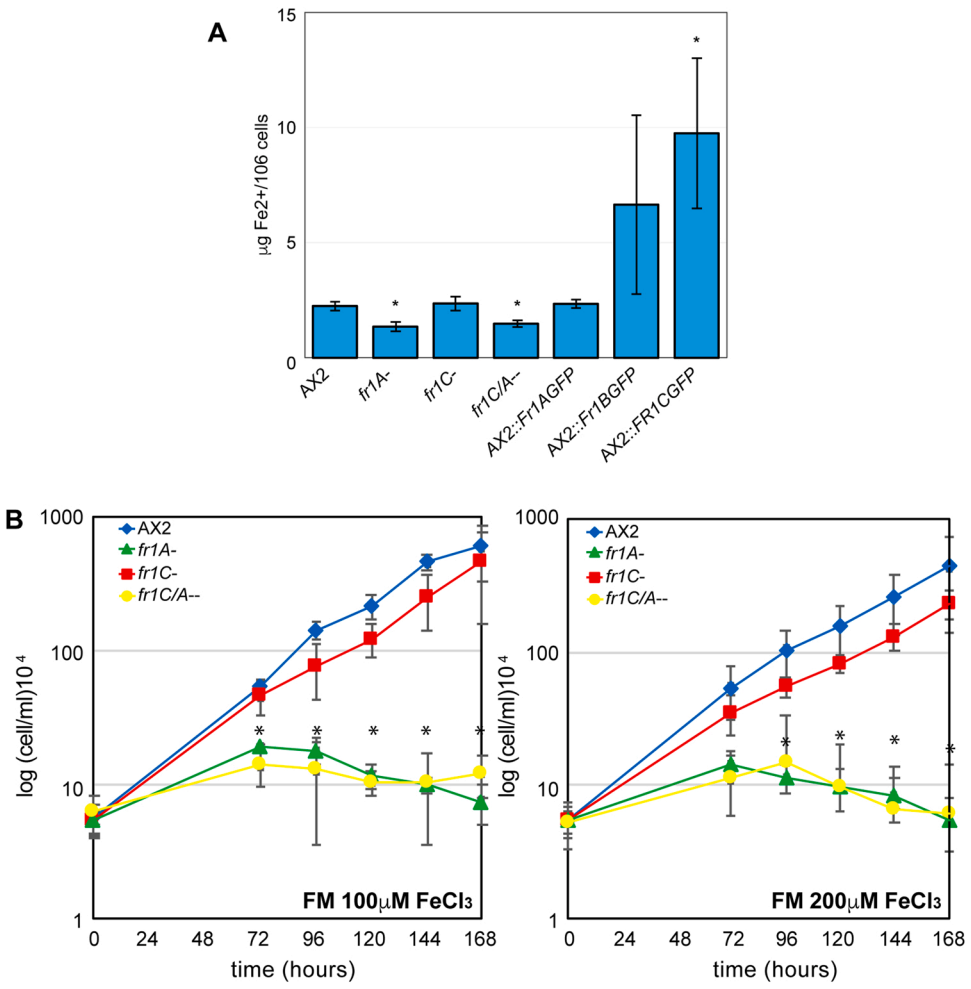

Fig. 9. Effects of single or double gene disruption on ferric reductase activity and on growth in minimal medium with standard or overload $FeCl_3$ supplementation. (A) Parental strain AX2; KO mutants (*fr1A-*; *fr1C-* and *fr1C/A–*) and overexpressing Fr1 cells (AX2:Fr1AGFP; AX2:Fr1BGFP and AX2:Fr1CGFP) were tested for the ability to reduce iron in a ferric reductase assay. Exponentially growing cells were washed free of medium and incubated at 23 °C in the dark in the presence of 0.1 mM $FeCl_3$. After the incubation cells were pelleted and to the supernatant was added NTA+Ferrozine and its absorbance was read at 562 nm. Data are the mean of four independent experiments. Statistically significant differences were determined by non-parametric t-test (* $P < 0.05$). (B) Exponentially growing cells were diluted in minimal medium with standard *(left)* or overloaded *(right)* $FeCl_3$ concentration, incubated under shaking and counted for growth at the indicated times. In the presence of 100 or 200 µM $FeCl_3$, *fr1A-* and *fr1C/A–* fail to grow whereas *fr1C-* grows with the same rate as parental strain AX2. Mean values of at least three experiments with SD. are shown. The asterisks denote significant difference (non-parametric t-test * $p < 0.05$) between AX2 versus the KO mutants *fr1A-* and *fr1C/A–*.

depends on deletion of fr1A, consistent with the very low expression of *fr1C* during growth (Fig. 1).

4. Discussion

Previous studies in our lab showed that the *Dictyostelium* iron transporter Nramp1, which is the ortholog of mammalian Nramp1, and confers resistance to pathogenic bacteria (Brenz et al., 2017; Peracino et al., 2013, 2006) is electrogenic and transports Fe^{2+} across the membrane of endo-lysosomal vesicles (Buracco et al., 2015b). To perform this function, Nramp1 needs to be coupled to a ferric reductase. In mammalian macrophages, a STEAP ferric reductase co-localizes with Nramp1 (Knutson, 2007). The *Dictyostelium* genome does not encode ferric reductases of the STEAP family but encodes three putative ferric chelate reductases belonging to the cytochrome b561 (Cyb561) protein family. The putative Dd Fr1 proteins (Fr1A, Fr1B, Fr1C) display five predicted transmembrane domains, the characteristic four conserved histidines residues, that are supposed to coordinate two heme molecules, and a N-terminus monooxygenase redox DOMON domain (Iyer et al., 2007). All three proteins harbor a signal peptide that may address them to the membranes of intracellular vesicles or plasma membranes.

The Cyb561s family generally functions as a monodehydroascorbate reductase, regenerating ascorbate, and as a ferric iron reductase, providing ferrous iron for TM transport (Su and Asard, 2006; Wyman et al., 2008). The *Dictyostelium* Fr1s do not contain conserved motives for binding ascorbate, suggesting that these putative ferric reductases utilize other electron donors.

Dd *fr1s* gene expression in the vegetative stage and early development highlights the importance of reducing iron to satisfy the need of metabolic energy during growth and aggregation. Overall, the strong increase in *fr1C* expression in the late post-aggregative phase could be linked to a potential need for ferric reductase in the germination phase, as it happens with homologous proteins in plants (Jeong and Guerinot, 2009; Muller et al., 2009), which are also phylogenetically closed to the *Dictyostelium* Fr1s.

We have shown that all three proteins localize with membranes of the endoplasmic reticulum, with Fr1B being exclusively in the ER. Fr1A, and to a much lower extent Fr1C, are additionally present in the Golgi and in acidic endolysosomal vesicles. Fr1C is also extensively located on the plasma membrane, like most CYDOMS plant proteins or SDR2 (the mouse Fr1), another Cyb561 protein that contains a DOMON domain on its N-terminus (Sun et al., 2009; Vargas et al., 2003). We took advantage of the plasma membrane associated Fr1CGFP fused protein to show, by means of Ferrozine assay, that the *Dictyostelium* Fr1s do indeed display ferric reductase activity.

The localization of the three Fr1 *like* proteins in the endoplasmic reticulum suggest a major role of iron in this compartment. Indeed, it has been shown that iron-proteins are especially enriched in endoplasmic reticulum and in mitochondria (Andreini et al., 2018).

To further strengthen such speculation an *in-silico* survey of the iron proteome in *Dictyostelium* confirms the presence of the three Dd Fr1 proteins in the group of Heme-family's proteins that are located mainly in the endoplasmic reticulum and in a little percentage in endosomes -unpublished data and (Andreini et al., 2018)-.

The co-localization of Fr1A and Fr1C in the membrane of macropinosomes, phagosomes and endo-lysosomal vesicles decorated with

Nramp1 and V-H^+ ATPase highlights the role of these ferric reductases for Nramp1-mediated ferrous iron transport across these vesicle membranes (Buracco et al., 2015b; Courville et al., 2006; Peracino et al., 2006).

Their dynamics of recruitment during engulfment of TRITC dextran or yeast particles and further intracellular traffic is very similar to what previously described for Nramp1 and for the V-H^+ ATPase (Peracino et al., 2006, 2010; Buracco et al., 2015b). Thereby, it is highly plausible to assume that these proteins work together in the same compartment, with Fr1C, and possibly also Fr1A, responsible for reducing Fe^{3+} and for Nramp1 mediating proton-coupled export to the cytoplasm of Fe^{2+}.

By using the biomarker FeRhonox-1, we have further shown that Fe^{2+} accumulates in endo-lysosomal vesicles positive for Fr1A, V-H^+-ATPase, and, at least in part, for Nramp1, confirming a role for Fr1A in ferric iron reduction and the involvement of V-H^+ ATPase in generating the electrogenic conditions to allow Fe^{2+} transport in the cytosol by Nramp1 (Buracco et al., 2015b). Ferhonox-1 is very likely taken up by (macro)pinocytosis and does not freely diffuse across intracellular membranes. Indeed, it has been shown to be selectively fluorescent in endolysosomal vesicles also in other cell types (Halcrow et al., 2019; Nash et al., 2019). Therefore, it is not surprising that the NrampB-positive contractile vacuole or the Calnexin-positive ER network failed to show Ferhonox-1 dependent fluorescence, despite the presence of all three ferric reductases in the ER. The lower Ferhonox-1 fluorescence in endosomes overexpressing Nramp1-GFP, when compared to endosomes positive for the vacuolar ATPase or Fr1A, may also be explained with the enhanced iron export activity of the overexpressed protein in these vesicles.

Single and double gene disruption was successful only for *fr1A* and *fr1C*, whereas no null mutants for *fr1B* could be selected, despite repeated attempts and screening of more than 450 clones. Consistently, we conclude that *fr1B* gene disruption is very likely lethal for *Dictyostelium* cell growth. Furthermore, the localization of Fr1B exclusively in the endoplasmic reticulum, and the finding that *fr1B* gene expression was strongly enhanced in the *fr1A* and *fr1C* null mutants suggest a crucial role for this ferric reductase in *Dictyostelium*. Although growth on bacteria was reduced in the null mutants, a compensatory role of Fr1B could mask a stronger effect of impaired ferric iron reduction on growth. Indeed, we showed previously that cell growth is very sensitive to iron deficiency or overload (Buracco et al., 2018, 2015b). In the developmental phase, the *fr1C* null mutant forms very large, sometimes multi-tipped streams, which undergo fragmentation, and displays a significant delay in fruiting body formation. Attempts to rescue this phenotype by overexpressing Fr1C-GFP was unsuccessful, while deleting also *fr1A* in the *fr1C* mutant restored the parental AX2 phenotype. On the other hand, both Fr1C-GFP and Fr1A-GFP overexpression altered the development of the parental AX2, by inducing in the first case a multi-tipped phenotype and in the second case by delaying post aggregative development. Noteworthy is also the mound flattening and the spiral and whirl movement effects of Fr1A-GFP on the *fr1A*- mounds. These results indicate that the GFP fused proteins are active, but their activity is affected by at least three variables, which may account for these manifold results: the differential expression/overexpression of the endogenous *fr1A* and *fr1B* in AX2 and in the single and double mutants, respectively, as shown in Fig. 3B; the constitutive expression of the GFP fused proteins under a strong promoter in cells where the endogenous proteins are differentially regulated during growth and development. Future experiments by expressing Fr1A and Fr1C under the control of their endogenous promoters as well as studying the effects of Fr1B-GFP expression in all strains may help dissecting these questions.

The large streams and multi-tipped phenotype occurring upon deletion of *fr1C*, but also upon overexpression of Fr1C-GFP in AX2, resemble that described for the Nramp1/ NrampB double knockout mutant (Peracino et al., 2010), for wild type cells grown in excess iron for several generations (Buracco et al., 2018), and recalls the streamer mutants, some of which are deficient in cGMP phosphodiesterase (Newell and Liu, 1992), suggesting a possible regulation of chemotaxis by iron homeostasis that needs further investigation. Interestingly both the cGMP phosphodiesterase (pdeD) and the cAMP/cGMP stimulated cAMP/cGMP phosphodiesterase (pdeE) are divalent metal binding proteins (Meima et al., 2003). Furthermore, in higher eukaryotes, the soluble guanylyl cyclase is regulated by the oxidative state of the heme cofactor (Fernhoff et al., 2012). Although *Dictyostelium* soluble guanylyl cyclase does not contain a heme binding domain (Schaap, 2005; Veltman et al., 2004) it would be interesting to know whether its activity is sensitive to iron. Mound flattening and spiral movements, resembling those observed in *fr1A*- overexpressing Fr1A-GFP, have also been described in aggregating cells and mounds and have been linked to factors regulating cAMP signaling (Rietdorf et al., 1997; Weijer, 1999), further strengthening the need of investigating potential links between iron homeostasis and chemotaxis.

Funding

This work was supported by a research grant of the Compagnia San Paolo/Università di Torino (12-CSP-C03-065) to SB, and intramural University of Torino funding to BP and VM (PERB_RILO_21_02; MONV_RILO_21_01).

Acknowledgements

We thank Annette Mueller Taubenberger for AX2 cells producing calnexin GFP and for the 389-2 vector (C-terminal mRFPmars); Markus Maniak for providing anti vatA and anti PDI antibodies; Hans Faix for the pLPBLP(floxed Bsr) and pDEX-NLS- cre plasmids; Marco Lo Iacono for help in generating Fr1A KO vector and Antonella Roetto for critical reading manuscript. We are grateful to the Dictybase team (www.dictybase.org) for maintenance of the Dictyostelid genome database.

Appendix A. Supporting information

Supplementary data associated with this article can be found in the online version at doi:10.1016/j.ejcb.2022.151230.

References

Andreini, C., Putignano, V., Rosato, A., Banci, L., 2018. The human iron-proteome. Metallomics 10, 1223–1231. https://doi.org/10.1039/c8mt00146d.

Asard, H., Barbaro, R., Trost, P., Bérczi, A., 2013. Cytochromes b561: ascorbate-mediated trans-membrane electron transport. Antioxid. Redox Signal. https://doi.org/10.1089/ars.2012.5065.

Ashworth, J.M., Watts, D.J., 1970. Metabolism of the cellular slime mould *Dictyostelium discoideum* grown in axenic culture. Biochem. J. 119, 175–182. https://doi.org/10.1042/bj1190175.

Barisch, C., Kalinina, V., Lefrançois, L.H., Appiah, J., Soldati, T., 2018. Think zinc: role of zinc poisoning in the intraphagosomal killing of bacteria by the amoeba Dictyostelium. bioRxiv. https://doi.org/10.1101/356949.

Bozzaro, S., Bucci, C., Steinert, M., 2008. Phagocytosis and host-pathogen interactions in Dictyostelium with a look at macrophages. Int. Rev. Cell Mol. Biol. 271, 253–300. https://doi.org/10.1016/S1937-6448(08)01206-9.

Bozzaro, S., Buracco, S., Peracino, B., 2013. Iron metabolism and resistance to infection by invasive bacteria in the social amoeba Dictyostelium discoideum. Front. Cell. Infect. Microbiol. https://doi.org/10.3389/fcimb.2013.00050.

Bozzaro, S., Buracco, S., Peracino, B., Eichinger, L., 2019. Dictyostelium host response to Legionella infection: strategies and assays. Methods Mol. Biol. https://doi.org/10.1007/978-1-4939-9048-1_23.

Brenz, Y., Ohnezeit, D., Winther-Larsen, H.C., Hagedorn, M., 2017. Nramp1 and NrampB contribute to resistance against Francisella in Dictyostelium. Front. Cell. Infect. Microbiol. 7. https://doi.org/10.3389/fcimb.2017.00282.

Buracco, S., Peracino, B., Andreini, C., Bracco, E., Bozzaro, S., 2018. Differential effects of iron, zinc, and copper on dictyostelium discoideum cell growth and resistance to Legionella pneumophila. Front. Cell. Infect. Microbiol. 7. https://doi.org/10.3389/fcimb.2017.00536.

Buracco, S., Peracino, B., Cinquetti, R., Signoretto, E., Vollero, A., Imperiali, F., Castagna, M., Bossi, E., Bozzaro, S., 2015b. Dictyostelium Nramp1, which is structurally and functionally similar tomammalian DMT1 transporter, mediates phagosomal iron efflux. J. Cell Sci. 128. https://doi.org/10.1242/jcs.173153.

Clarke, M., Maddera, L., Engel, U., Gerisch, G., 2010. Retrieval of the vacuolar H-ATPase from phagosomes revealed by live cell imaging. PLoS One 5, e8585. https://doi.org/10.1371/journal.pone.0008585.

Courville, P., Chaloupka, R., Cellier, M.F.M., 2006. Recent progress in structure-function analyses of Nramp proton-dependent metal-ion transporters. Biochem. Cell Biol. 84, 960–978. https://doi.org/10.1139/o06-193.

Dunn, L.L., Rahmanto, Y.S., Richardson, D.R., 2007. Iron uptake and metabolism in the new millennium. Trends Cell Biol. https://doi.org/10.1016/j.tcb.2006.12.003.

Faix, J., Kreppel, L., Shaulsky, G., Schleicher, M., Kimmel, A.R., 2004. A rapid and efficient method to generate multiple gene disruptions in Dictyostelium discoideum using a single selectable marker and the Cre-loxP system. Nucleic Acids Res. 32, e143 https://doi.org/10.1093/nar/gnh136.

Fernhoff, N.B., Derbyshire, E.R., Underbakke, E.S., Marletta, M.A., 2012. Heme-assisted S-nitrosation desensitizes ferric soluble guanylate cyclase to nitric oxide. J. Biol. Chem. 287, 43053–43062. https://doi.org/10.1074/jbc.M112.393892.

Fischer, M., Haase, I., Simmeth, E., Gerisch, G., Müller-Taubenberger, A., 2004. A brilliant monomeric red fluorescent protein to visualize cytoskeleton dynamics in Dictyostelium. FEBS Lett. 577, 227–232. https://doi.org/10.1016/j.febslet.2004.09.084.

Fok, A.K., Clarke, M., Ma, L., Allen, R.D., 1993. Vacuolar H(+)-ATPase of Dictyostelium discoideum. A monoclonal antibody study. J. Cell Sci. 106 (Pt 4), 1103–1113.

Franke, J., Kessin, R., 1977. A defined minimal medium for axenic strains of Dictyostelium discoideum. Proc. Natl. Acad. Sci. USA 74, 2157–2161. https://doi.org/10.1073/pnas.74.5.2157.

Gao, G., Li, J., Zhang, Y., Chang, Y.-Z., 2019. Cellular Iron Metabolism and Regulation, pp. 21–32. https://doi.org/10.1007/978-981-13-9589-5_2.

Halcrow, P., Khan, N., Datta, G., Ohm, J.E., Chen, X., Geiger, J.D., 2019. Importance of measuring endolysosome, cytosolic, and extracellular pH in understanding the pathogenesis of and possible treatments for glioblastoma multiforme. Cancer Rep. 2. https://doi.org/10.1002/cnr2.1193.

Hanna, N., Koliwer-Brandl, H., Lefrançois, L.H., Kalinina, V., Cardenal-Muñoz, E., Appiah, J., Leuba, F., Gueho, A., Hilbi, H., Soldati, T., Barisch, C., 2021. Zn2+ intoxication of Mycobacterium marinum during Dictyostelium discoideum infection is counteracted by induction of the pathogen Zn2+ exporter CtpC. mBio 12. https://doi.org/10.1128/mBio.01313-20.

Hirayama, T., Nagasawa, H., 2017. Chemical tools for detecting Fe ions. J. Clin. Biochem. Nutr. 60, 39–48. https://doi.org/10.3164/jcbn.16670.

Hirayama, T., Okuda, K., Nagasawa, H., 2013. A highly selective turn-on fluorescent probe for iron(ii) to visualize labile iron in living cells. Chem. Sci. 4, 1250–1256. https://doi.org/10.1039/c2sc21649c.

Hirschhorn, T., Stockwell, B.R., 2019. The development of the concept of ferroptosis. Free Radic. Biol. Med. 133, 130–143. https://doi.org/10.1016/j.freeradbiomed.2018.09.043.

Iyer, L.M., Anantharaman, V., Aravind, L., 2007. The DOMON domains are involved in heme and sugar recognition. Bioinformatics 23, 2660–2664. https://doi.org/10.1093/bioinformatics/btm411.

Jeong, J., Guerinot, M. lou, 2009. Homing in on iron homeostasis in plants. Trends Plant Sci. https://doi.org/10.1016/j.tplants.2009.02.006.

Kawabata, H., 2019. Transferrin and transferrin receptors update. Free Radic. Biol. Med. https://doi.org/10.1016/j.freeradbiomed.2018.06.037.

Kay, R.R., 2021. Macropinocytosis: biology and mechanisms. Cells Dev., 203713 https://doi.org/10.1016/j.cdev.2021.203713.

Kimmel, A.R., Faix, J., 2006. Generation of multiple knockout mutants using the Cre-loxP system. Methods Mol. Biol. 346, 187–199. https://doi.org/10.1385/1-59745-144-4:187.

Knutson, M.D., 2007. Steap proteins: implications for iron and copper metabolism. Nutr. Rev. 65, 335–340. https://doi.org/10.1111/j.1753-4887.2007.tb00311.x.

Meima, M.E., Weening, K.E., Schaap, P., 2003. Characterization of a cAMP-stimulated cAMP phosphodiesterase in Dictyostelium discoideum. J. Biol. Chem. 278, 14356–14362. https://doi.org/10.1074/jbc.M209648200.

Monnat, J., Hacker, U., Geissler, H., Rauchenberger, R., Neuhaus, E.M., Maniak, M., Soldati, T., 1997. Dictyostelium discoideum protein disulfide isomerase, an endoplasmic reticulum resident enzyme lacking a KDEL-type retrieval signal. FEBS Lett. 418, 357–362. https://doi.org/10.1016/s0014-5793(97)01415-4.

Muckenthaler, M.U., Rivella, S., Hentze, M.W., Galy, B., 2017. A red carpet for iron metabolism. Cell. https://doi.org/10.1016/j.cell.2016.12.034.

Muller, K., Linkies, A., Vreeburg, R.A.M., Fry, S.C., Krieger-Liszkay, A., Leubner-Metzger, G., 2009. In vivo cell wall loosening by hydroxyl radicals during cress seed germination and elongation growth. Plant Physiol. 150, 1855–1865. https://doi.org/10.1104/pp.109.139204.

Müller-Taubenberger, A., Lupas, A.N., Li, H., Ecke, M., Simmeth, E., Gerisch, G., 2001. Calreticulin and calnexin in the endoplasmic reticulum are important for phagocytosis. EMBO J. 20, 6772–6782. https://doi.org/10.1093/emboj/20.23.6772.

Nash, B., Tarn, K., Irollo, E., Luchetta, J., Festa, L., Halcrow, P., Datta, G., Geiger, J.D., Meucci, O., 2019. Morphine-induced modulation of endolysosomal iron mediates upregulation of ferritin heavy chain in cortical neurons. ENEURO.0237-19.2019 eneuro 6. https://doi.org/10.1523/ENEURO.0237-19.2019.

Newell, P.C., Liu, G., 1992. Streamer F mutants and chemotaxis of Dictyostelium. Bioessays 14, 473–479. https://doi.org/10.1002/bies.950140708.

Ohgami, R.S., Campagna, D.R., McDonald, A., Fleming, M.D., 2006. The steap proteins are metalloreductases. Blood 108, 1388–1394. https://doi.org/10.1182/blood-2006-02-003681.

Pang, K.M., Lynes, M.A., Knecht, D.A., 1999. Variables controlling the expression level of exogenous genes in Dictyostelium. Plasmid 41, 187–197. https://doi.org/10.1006/plas.1999.1391.

Parkinson, K., Baines, A.E., Keller, T., Gruenheit, N., Bragg, L., North, R.A., Thompson, C. R.L., 2014. Calcium-dependent regulation of Rab activation and vesicle fusion by an intracellular P2X ion channel. Nat. Cell Biol. 16, 87–98. https://doi.org/10.1038/ncb2887.

Peracino, B., Balest, A., Bozzaro, S., 2010. Phosphoinositides differentially regulate bacterial uptake and Nramp1-induced resistance to Legionella infection in Dictyostelium. J. Cell Sci. 123. https://doi.org/10.1242/jcs.072124.

Peracino, B., Borleis, J., Jin, T., Westphal, M., Schwartz, J.-M., Wu, L., Bracco, E., Gerisch, G., Devreotes, P., Bozzaro, S., 1998. G protein β subunit-null mutants are impaired in phagocytosis and chemotaxis due to inappropriate regulation of the actin cytoskeleton. J. Cell Biol. 141. https://doi.org/10.1083/jcb.141.7.1529.

Peracino, B., Buracco, S., Bozzaro, S., 2013. The Nramp (Slc11) proteins regulate development, resistance to pathogenic bacteria and iron homeostasis in Dictyostelium discoideum. J. Cell Sci. 126, 301–311. https://doi.org/10.1242/jcs.116210.

Peracino, B., Wagner, C., Balest, A., Balbo, A., Pergolizzi, B., Noegel, A.A., Steinert, M., Bozzaro, S., 2006. Function and mechanism of action of Dictyostelium Nramp1 (Slc11a1) in bacterial infection. Traffic 7. https://doi.org/10.1111/j.1600-0854.2005.00356.x.

Rietdorf, J., Siegert, F., Dharmawardhane, S., Firtel, R.A., Weijer, C.J., 1997. Analysis of cell movement and signalling during ring formation in an activated G alpha1 mutant of Dictyostelium discoideum that is defective in prestalk zone formation. Dev. Biol. 181, 79–90. https://doi.org/10.1006/dbio.1996.8447.

Rosengarten, R.D., Santhanam, B., Fuller, D., Katoh-Kurasawa, M., Loomis, W.F., Zupan, B., Shaulsky, G., 2015. Leaps and lulls in the developmental transcriptome of Dictyostelium discoideum. BMC Genom. 16, 294. https://doi.org/10.1186/s12864-015-1491-7.

Schaap, P., 2005. Guanylyl cyclases across the tree of life. Front. Biosci. 10, 1485–1498. https://doi.org/10.2741/1633.

Sillo, A., Bloomfield, G., Balest, A., Balbo, A., Pergolizzi, B., Peracino, B., Skelton, J., Ivens, A., Bozzaro, S., 2008. Genome-wide transcriptional changes induced by phagocytosis or growth on bacteria in Dictyostelium. BMC Genom. 9, 291. https://doi.org/10.1186/1471-2164-9-291.

Stajdohar, M., Rosengarten, R.D., Kokosar, J., Jeran, L., Blenkus, D., Shaulsky, G., Zupan, B., 2017. dictyExpress: a web-based platform for sequence data management and analytics in Dictyostelium and beyond. BMC Bioinform. 18, 291. https://doi.org/10.1186/s12859-017-1706-9.

Steinert, M., 2011. Pathogen-host interactions in Dictyostelium, Legionella, Mycobacterium and other pathogens. Semin. Cell Dev. Biol. 22, 70–76. https://doi.org/10.1016/j.semcdb.2010.11.003.

Su, D., Asard, H., 2006. Three mammalian cytochromes b561 are ascorbate-dependent ferrireductases. FEBS J. 273, 3722–3734. https://doi.org/10.1111/j.1742-4658.2006.05381.x.

Sultana, H., Rivero, F., Blau-Wasser, R., Schwager, S., Balbo, A., Bozzaro, S., Schleicher, M., Noegel, A.A., 2005. Cyclase-associated protein is essential for the functioning of the endo-lysosomal system and provides a link to the actin cytoskeleton. Traffic 6, 930–946. https://doi.org/10.1111/j.1600-0854.2005.00330.x.

Sun, Q., Zybailov, B., Majeran, W., Friso, G., Olinares, P.D.B., van Wijk, K.J., 2009. PPDB, the plant proteomics database at Cornell. Nucleic Acids Res. 37. https://doi.org/10.1093/nar/gkn654.

Tsubaki, M., Takeuchi, F., Nakanishi, N., 2005. Cytochrome b561 protein family: expanding roles and versatile transmembrane electron transfer abilities as predicted by a new classification system and protein sequence motif analyses. Biochim. Biophys. Acta Proteins Proteom. 1753, 174–190. https://doi.org/10.1016/j.bbapap.2005.08.015.

Vargas, J.D., Herpers, B., McKie, A.T., Gledhill, S., McDonnell, J., van den Heuvel, M., Davies, K.E., Ponting, C.P., 2003. Stromal cell-derived receptor 2 and cytochrome b561 are functional ferric reductases. Biochim. Biophys. Acta Proteins Proteom. 1651, 116–123. https://doi.org/10.1016/S1570-9639(03)00242-5.

Veltman, D.M., Bosgraaf, L., van Haastert, P.J.M., 2004. Unusual guanylyl cyclases and cGMP signaling in Dictyostelium discoideum. Vitam. Horm. 69, 95–115. https://doi.org/10.1016/S0083-6729(04)69004-2.

Weijer, C.J., 1999. Morphogenetic cell movement in Dictyostelium. Semin. Cell Dev. Biol. 10, 609–619. https://doi.org/10.1006/scdb.1999.0344.

Weiner, O.H., Murphy, J., Griffiths, G., Schleicher, M., Noegel, A.A., 1993. The actin-binding protein comitin (p24) is a component of the Golgi apparatus. J. Cell Biol. 123, 23–34. https://doi.org/10.1083/jcb.123.1.23.

Westphal, M., Jungbluth, A., Heidecker, M., Mühlbauer, B., Heizer, C., Schwartz, J.M., Marriott, G., Gerisch, G., 1997. Microfilament dynamics during cell movement and chemotaxis monitored using a GFP-actin fusion protein. Curr. Biol. 7, 176–183. https://doi.org/10.1016/s0960-9822(97)70088-5.

White, C., Yuan, X., Schmidt, P.J., Bresciani, E., Samuel, T.K., Campagna, D., Hall, C., Bishop, K., Calicchio, M.L., Lapierre, A., Ward, D.M., Liu, P., Fleming, M.D., Hamza, I., 2013. HRG1 is essential for heme transport from the phagolysosome of macrophages during erythrophagocytosis. Cell Metab. 17, 261–270. https://doi.org/10.1016/j.cmet.2013.01.005.

Williams, T.D., Kay, R.R., 2018. The physiological regulation of macropinocytosis during Dictyostelium growth and development. J. Cell Sci. 131. https://doi.org/10.1242/jcs.213736.

Wyman, S., Simpson, R.J., McKie, A.T., Sharp, P.A., 2008. Dcytb (Cybrd1) functions as both a ferric and a cupric reductase in vitro. FEBS Lett. 582, 1901–1906. https://doi.org/10.1016/j.febslet.2008.05.010.

Yanatori, I., Kishi, F., 2019. DMT1 and iron transport. Free Radic. Biol. Med. https://doi.org/10.1016/j.freeradbiomed.2018.07.020.